Transparent and colorless DSSC featuring thienyl-pyrrolopyrrole cyanine sensitizers

Thibaut Baron, Waad Naim, Mate Kurucz, Ilias Nikolinakos, Baptiste Andrin, Yann Pellegrin, Denis Jacquemin, Stefan Haacke, Frédéric Sauvage, Fabrice Odobel

ARTICLE

Transparent and colorless DSSC featuring thienyl-pyrrolopyrrole cyanine sensitizers

Received 00th January 20xx,
Accepted 00th January 20xx

DOI: 10.1039/x0xx00000x

Thibaut Baron,[a#] Waad Naim,[b#] Mate Kurucz,[c] Ilias Nikolinakos,[c#] Baptiste Andrin,[a] Yann Pellegrin,[a] Denis Jacquemin,[*a,d] Stefan Haacke,[*c] Frédéric Sauvage,[*b] and Fabrice Odobel[*a]

Fully transparent and colorless Dye Sensitized Solar Cells have recently gained much attention due to their unconventional properties. Following the known strategy to redshift the absorption band of diketopyrrolopyrrole chromophores that consists in substituting phenyl rings by thiophene, we propose herein to extend that procedure to pyrrolopyrrole cyanine in order to prepare new thienyl-*PPcy* dyes. These new dyes were investigated by UV-vis absorption and emission spectroscopy, by electrochemistry, and their electronic properties were rationalized by DT-DFT calculations. A significant bathochromic shift (30 nm) was observed compared to previous *PPcy* allowing to reach a better Average Visible Transmittance of 67%. A detailed photophysical study demonstrates that the lower performances are due to a stronger aggregation tendency and a slower electron injection rate connected with a lower driving force inducing a higher quenching degree by energy transfer towards the aggregates. This study reveals the great potential of this type of dyes for TPV because these drawbacks could be circumvented by molecular engineering of new *PPcys-th*.

Introduction

Sunlight offers a suitable alternative to fossil fuels in order to cope with the increasing energy consumption and global warming.[1] Projects to harness solar energy have already contributed to the electricity production with *c.a.* 700 GW of installed solar panels. However, more than 90% of the deployed photovoltaic devices are still based on poly- and mono-crystalline silicon technologies and their implementation in buildings- usually referred to as Building Integrated Photovoltaic (BIPV)[2] is essentially limited to roofs. Over the past decade, many efforts were made to develop transparent photovoltaic (TPV) systems,[3] that would permit to broaden their integration for instance as windows in buildings, in cars or even in greenhouses.[4] In fact, it is tantalizing to imagine integrated transparent solar panels in windows to generate electric power while retaining natural lighting. In addition to the power conversion efficiency (PCE), the two other key figures of merit of TPV are the average visible transmittance (AVT) and the color rendering index (CRI). Light Utilization Efficiency (LUE) has been also introduced as the product of PCE and AVT (LUE= PCExAVT), enabling the comparison between technologies against theoretical limits.[8] This is especially true when paralleling semi-transparent PV technologies which can have high AVT but very low CRI and high LUE values in spite of this. By contrast, TPV technologies combine high AVT and CRI, therefore excellent aesthetic characteristics but low LUE values because so far PCE still need improvements. It is agreed upon that an AVT of at least 55% and a CRI equal or larger to 90 are sufficient for reaching a satisfying visual perception.[5,6] Two main strategies, based on wavelength and non-wavelength selective absorption of the visible light, are currently used to develop TPV systems. Non-wavelength selective TPV technologies mostly focus on inorganic semiconductors and perovskite solar cells,[7] and rely on the reduction of the thickness of the active layer or the drilling of holes into the devices. However, this strategy does not allow to reach high AVT and LUE values, because the PCE drops to 0% when AVT tends to 100%; moreover the panels are still intensely coloured.[8] The second approach, that is the selective absorption of UV and/or IR light is the other attractive strategy to obtain highly transparent photovoltaic devices. It presents the great advantages to theoretically reach 20.6% PCE combined with a 100% AVT.[8] In this framework, it has been shown that the DSSC (Dye Sensitized Solar Cell) technology presents the appropriate characteristics for TPV and consequently appears to be an appealing candidate for this application.[9] In fact, DSSCs are potentially cheap to manufacture, present relatively good stability, are naturally semi-transparent and the final color can be easily tuned by modifying the photosensitizer in order to obtain the desired aesthetics properties.[10] Nevertheless, the most efficient dyes employed in DSSCs absorb in the visible region (between 400-700 nm) and there are relatively few

[a] *Université de Nantes, CNRS, CEISAM UMR 6230, F-44000 Nantes, France. E-mail: Fabrice.Odobel@univ-nantes.fr and denis.jacquemin@univ-nantes.fr*
[b] *Laboratoire de Réactivité et Chimie des Solides, Université de Picardie Jules Verne (UPJV), CNRS UMR 7314, 80039 Amiens, France; E-mail: frederic.sauvage@u-picardie.fr*
[c] *Université de Strasbourg – CNRS, IPCMS, UMR 7504, 67034 Strasbourg, France. E-mail: stefan.haacke@ipcms.unistra.fr*
[d] *Institut Universitaire de France (IUF), F-75005 Paris, France.:*
#these authors equally contributed to this study† Footnotes relating to the title and/or authors should appear here.
Electronic Supplementary Information (ESI) available: [details of any supplementary information available should be included here]. See DOI: 10.1039/x0xx00000x

sensitizers exploiting low energy photon (above 750 nm).[10] Among them, some ruthenium[11] and osmium complexes,[12] metal-free organic dyes,[13,14] porphyrins[15] and BODIPY[16] derivatives exhibit Incident-Photon-to-electron Conversion Efficiency (IPCE) in the NIR region till 1000 nm. In order to prepare colorless DSSC, it is necessary to avoid photon absorption in the visible region. In this context, Zhang *et al.* published in 2014 the first wavelength-selective DSSC for see-through photovoltaic applications by co-sensitization of two selective UV and NIR dyes, coded **Y1** and **HSQ5**, respectively, leading to a highly transparent solar cell with a maximum transmittance of 60.3% combined to a 3.66% PCE.[17] Even though a good transparency was achieved, the final device still retained an intense green/yellow coloration. More recently, Sauvage *et coll.* reported the cyanine **VG20** exhibiting an absorption maximum at 834 nm and providing a 3.10% PCE with a scattering layer.[18] Without the scattering layer, the PCE reaches 2.4% with an AVT value up to 76% when the $Co(bpy)_3^{3+/2+}$ redox mediator is used in the electrolyte, leading to a pleasantly aesthetic solar cell (CRI = 92.1). More recently, we have shown the potential of zinc phthalocyanine and pyrrolopyrrole cyanine dyes as colorless sensitizers for DSSC.[19] For example, the pyrrolopyrrole cyanine **TB207** outperforms **VG20** as it provides a PCE reaching 2.5% under AM 1.5, with an AVT of 76% and a CRI of 93.[20] However, this dye is still limited by a relatively low electron injection driving force and the final device presents a slightly green coloration. In order to solve these issues, we explore the possibility to raise the HOMO and LUMO levels of this family of dyes. To this end, we investigate the substitution of the phenyl ring by a thienyl on the bispyrrole unit for the development of more electron rich pyrrolopyrrole cyanine dyes with the possible consequence to redshift the main absorption band in the NIR. Indeed, it was shown that the replacement of phenyl by thienyl units in diketopyrrolopyrrole (*DPP*) induces a significant redshift of the absorption band, an increase of the extinction molar coefficient and renders the dye easier to oxidize.[21,22] Until the very recent paper of Zhang and co-workers,[23] published during the preparation of this article, there was no report of thienyl substituted pyrrolopyrrole cyanine (*PPcy*).

Herein, we report the synthesis and the characterizations of two new pyrrolopyrrole cyanine dyes **TB179** and **TB202**, analogues of **TB144** and **TB207**, but substituted by thienyl units instead of phenyl moieties on the bispyrrole core (*PPcys-th*) (Chart). The properties of these dyes are directly compared to previous *PPcys* to notify the impact of thienyl introduction into the *PPcy* derivatives on spectroscopic and electrochemical properties. This study shows that *PPcys-th* are more transparent than *PPcys* and reach 67% of AVT with a PCE of 1.5% essentially limited by the higher propensity to aggregate on TiO_2 surface and by a lower electron injection rate constant than **TB207**.

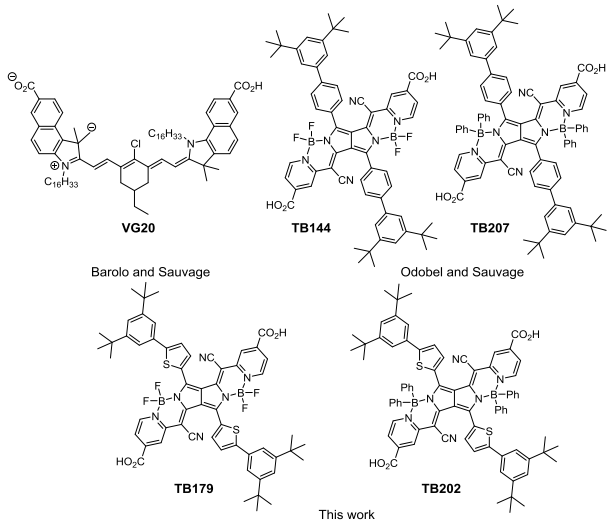

Chart. Structures of previously published NIR dyes for transparent DSSCs and the new sensitizers **TB179** and **TB202** investigated in this study.

Synthesis

Following the strategy for the preparation of previously described *PPcys* **TB144** and **TB207**,[20] the synthesis of sensitizers **TB179** and **TB202** requires the soluble thienyl diketopyrrolopyrrole **3**. This intermediate is obtained by Suzuki cross-coupling reaction between the pinacol ester **2** and dibromo thiophene *N*-Boc **1**, whose synthesis has already been described by Yang et al. (Scheme 1).[24] The desired N-H soluble *DPP* **3** was obtained with a moderate yield of 54%, which can be attributed to high temperature sensitivity of **1**. After activation with $POCl_3$, the *DPP* **3** was then engaged in the subsequent condensation step involving the pyridine acetonitrile derivative **4**. The symmetrical H-*PPcy* **5** was isolated with a 43% yield, which is consistent with the previous parent *PPcy* containing phenyl ring on bipyrrole core.[25] Indeed, the thienyl moiety does not affect the chemistry to form the *PPcy*.

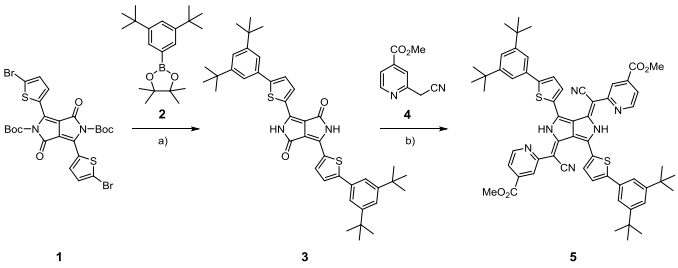

Scheme 1. Synthetic route to pyrrolopyrrole cyanine thienyl **5**. Reagents and conditions: a) **2**, K_2CO_3, $Pd(PPh_3)_4$, THF/H_2O : 3/1, 80°C, 16h, 54%; b) $POCl_3$, Toluene, 130°C, 2 h, 43%.

Pyrrolopyrrole cyanines contain nitrogen atoms that can be complexed by a boron atom similarly to BODIPY[26] and aza-BODIPY dyes.[27]

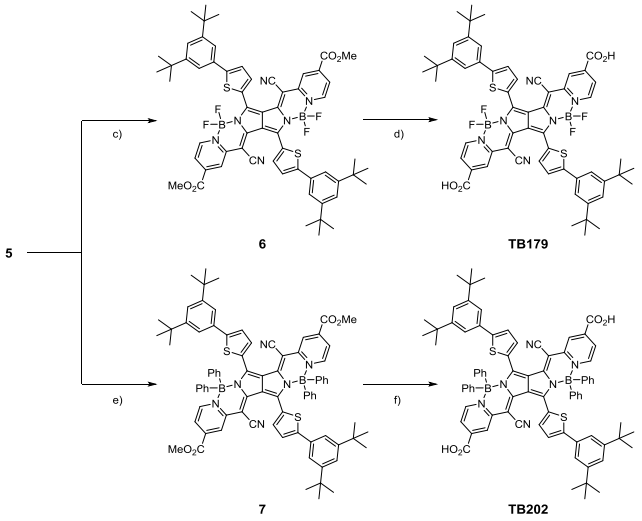

Scheme 2. Synthetic route to thienyls pyrrolopyrrole cyanine **TB179** and **TB202**. Reagents and conditions: c) $BF_3.OEt_2$, DIPEA, CH_2Cl_2, 45°C, 30 min., 100%; d) LiOH, THF/H_2O, rt, 2h, 72%; e) $B(Ph)_2Cl$, DIPEA, CH_2Cl_2, 45°C, 30min, 26%; f) LiOH, THF/H_2O, rt, 2h, 87%.

Following the procedure described by Fisher et al.,[28] *PPcy* **5** was chelated by boron with BF_3-OEt_2 with a quantitative yield, while **7** was reacted with $B(Ph)_2Cl$ leading to **7** with 26% yield. This lower yield can be attributed to the high sensitivity of boron precursor ($B(Ph)_2Cl$) to moisture. Finally, the ester groups on both *PPcy-th* **6** and **7** were saponified under mild basic conditions to afford the desired photosensitizers **TB179** and **TB202** in high yields (Scheme 2).[29]

UV-Visible absorption and emission spectra

TB179 and **TB202** absorption and emission spectra were recorded in dimethylformamide solution at room temperature (Figure 1a). The optical data including wavelengths of maximal absorption (λ_{abs}), extinction coefficients (ε), wavelength of maximal emission (λ_{em}) and zero-zero energy level of the lowest singlet excited state ($E_{0\text{-}0}$), are collected in Table 1.

Both **TB179** and **TB202** dyes exhibit an intense and thin absorption band corresponding to π-π* transitions at 735 and 789 nm respectively, and a weaker absorption band at 676 and 710 nm corresponding to vibronic overtone (Figure 1a).[25] The absorption bands display the classical features of pyrrolopyrrole cyanine dyes, and show that the thienyl unit does not drastically modify the spectroscopic features. The strong influence of the substituents on the boron centers is confirmed on **TB179** and **TB202**, where the substitution of fluorine by phenyl induces a significant redshift of the absorption maxima (+ 60 nm). This is mainly attributed to the electron donating effect of the thiophenes that increases the HOMO energy level (see below for DFT calculations and electrochemistry). As expected, the optical spectra of both dyes **TB179** and **TB202** are redshifted compared to previous *PPcy* **TB144** and **TB207** (≈ 30 nm).[20] In fact, the thienyl group stabilizes the LUMO level causing a decrease of the 0-0 energies. This shift is lower compared to *DPP* derivatives, with values around 60 nm, but confirms the positive impact of thienyl in order for tuning and red-shifting the absorption of *PPcy* dyes.

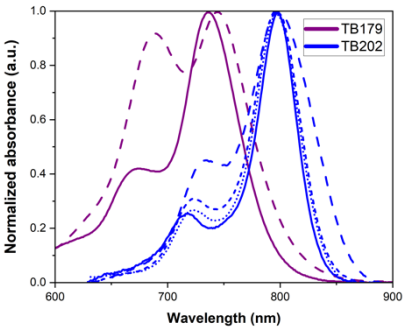

(a)

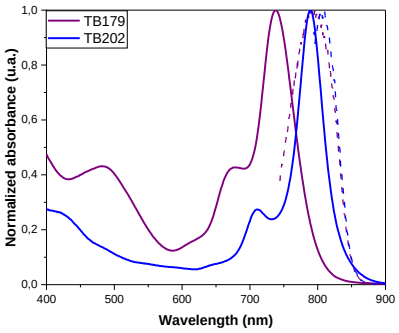

(b)

Figure 1. a) Normalized absorption (solid line) and emission (dashed line) spectra of **TB179** (purple line) and **TB202** (blue line) recorded in dimethylformamide solution at room temperature, b) Normalized absorption spectra recorded in DMF solution (solid line) and on thin TiO_2 films (dashed/dotted lines) with **TB179** (purple) or **TB202** (blue). The CDCA concentration is 50 mM for **TB179,** and for **TB202**, concentrations are 0, 10 and 30 mM (dashed, short-dashed and dotted). For increasing CDCA concentrations a

clear reduction of the aggregate absorption is observed (low energy tail, and increased absorbance at 700-750 nm).

Moreover, **TB179** and **TB202** exhibit weak absorption in the visible range (450-550 nm) leading to a colour change from green (for classical *PPcys*) to purple (Figure S1). Interestingly, **TB202** presents suitable spectroscopic properties for the development of transparent and colourless dye sensitized solar cells with almost no absorption in the 450-700 nm range.
Our previous study showed the propensity of *PPcy* dyes to aggregate on TiO_2 surface.[20] Aggregates are well-known to limit the injection process by quenching the dye excited state.[30] To prevent aggregation a co-adsorbent such as chenodeoxycholic acid (CDCA) is typically added in the dyeing bath.[31] Absorption spectra of **TB179** and **TB202** co-adsorbed on TiO_2 with low-to-high concentrations of CDCA were recorded (Figure 1b). **TB179** presents an important degree of aggregation, even at the highest CDCA concentration (c = 50 mM, dye-to-CDCA ratio 1:500). The width of the bands and the absorption of around 680 nm, *i.e.* below the monomer absorption peak, is increased on TiO_2 compared to the solution, indicating the presence of aggregates. On the contrary, for **TB202**, compared to the aggregate-free solution spectrum, a clear reduction of the aggregate features is observed (less broadening for λ> 800 nm, and decreased absorbance at 700-750 nm), as the CDCA concentration increases. These results highlight the strong influence of substituents on boron, with the phenyl rings increasing the steric hindrance and hampering π-π stacking for **TB202**.
Both **TB179** and **TB202** dyes are fluorescent and exhibit emission maxima at 756 and 803 nm respectively, enabling us to calculate the $E_{0\text{-}0}$, which was estimated to 1.66 and 1.56 eV (Table 1). The $E_{0\text{-}0}$ value calculated for **TB202** represents one of the lowest value recorded for pyrrolopyrrole cyanine dyes.[32]

Table 1. Wavelength of maximal absorption (λ_{abs}), maximal emission (λ_{em}) and emission lifetime (τ_{em}) recorded at room temperature in dichloromethane and zero-zero energy level of the lowest excited state ($E_{0\text{-}0}$).

Dye	λ_{abs} [nm]	λ_{em} [nm]	τ_{em} [ns]	$E_{0\text{-}0}$/eV[a]
TB179	735	756	0.79	1.66
TB202	789	803	0.88	1.56

[a]calculated with $E_{0\text{-}0}$= 1240 eV/λ_{inter}, with λ_{inter}= wavelength (in nm) at the intersection of the normalized absorption and emission spectra.

Electrochemical measurements

The oxidation potentials of **TB179** and **TB202** were determined by cyclic voltammetry in dimethylformamide solution with Bu_4NPF_6 as supporting salt (Figure S2 and S3). Both free Gibbs energies for electron injection ($\Delta G°_{inj}$) into the TiO_2 conduction band and dye regeneration ($\Delta G°_{reg}$) with I_3^-/I^- redox couple were calculated and summarized in Table 2. **TB179** exhibits a non-reversible oxidation wave at 1.10 V *vs.* SCE corresponding to the formation of the radical cation. At the same scan rate, **TB202** presents a quasi-reversible oxidation wave at 0.84 V *vs.* SCE. The difference of reversibility can be attributed to the radical cation stability[33] which is more stable for **TB202** than **TB179** owing to its lower potential. Such behaviour has already been observed on BODIPY derivatives.[34] In addition, **TB202** is oxidized at a more cathodic potential than **TB179** (ΔE = 260 mV), indicating that phenyl substituents on boron increase the HOMO level. However, the substitution of phenyl by thienyl on bispyrrole core does not affect the reducing strength in the excited state, in line with DFT calculations (see below). Indeed, the oxidation potential of **TB202** is similar within experimental error to that of **TB207** (0.82 V *vs.* SCE).[20] The excited states of both **TB179** and **TB202** dyes are less electron donating compared to the previously reported **TB144** and **TB207** *PPcy* dyes owing to a decrease of the excited state energy level (Table 2). Consequently, the driving force ($\Delta G°_{inj}$ = 0.16 eV for **TB179** and -0.02 eV for **TB202**) are not sufficiently large to ensure a high electron injection efficiency (see photophysical study below).[35]

Table 2. Redox potentials recorded by cyclic voltammetry at room temperature in dimethylformamide solution with Bu_4NPF_6 (0.1M) as supported electrolyte and referenced versus saturated calomel electrode (SCE). Calculated Gibbs free energies for electron injection ($\Delta G°_{inj}$) and dye regeneration ($\Delta G°_{reg}$).

Dye	E (S^+/S) [V vs. SCE]	E (S^+/S^*) [V vs. SCE]	[a]$\Delta G°_{inj}$ [eV]	[b]$\Delta G°_{reg}$ (I^-/I_3^-) [eV]
TB179	1.10	-0.56	0.16	-1.0
TB202	0.84	- 0.72	- 0.02	-0.74

[a]calculated with the equation: $\Delta G°_{inj}$ = (E (S^+/S) – $E_{0\text{-}0}$) - $E_{CB}(TiO_2)$ with $E_{CB}(TiO_2)$ = -0.7 V vs. SCE.[b]calculated with the equation: $\Delta G°_{reg}$ = E(M^+/M) - E (S^+/S), with M= redox mediator and E(I_3^-/I^-) = 0.1 V *vs.* SCE.

However, it has been shown for a previous cyanine[18] and *PPcy*[20] sensitizers that a high concentration of potential determining lithium salt in the electrolyte would favour the electron injection process because the conduction band of TiO_2 is bent downwards. On the other hand, the regeneration of both oxidized *PPcys-th* **TB179** and **TB202** by iodide is thermodynamically very favourable since the $\Delta G°_{reg}$ values are -1.0 and -0.74 eV respectively.[36]

Computational study

Time-Dependent Density Functional Theory (TD-DFT) calculations were performed on both **TB179** and **TB202**, using a protocol that is detailed in the ESI. Both the ground (S_0) and excited (S_1) state geometries of the two structures are true minima in the C_i point group. The lowest excited states are bright (dipole-allowed) A_u with transition wavelengths above 650 nm (see Table S1). The next states are either A_u (but low oscillator strengths) or symmetry-forbidden A_g states. In **TB179**, TD-DFT foresees a significant absorption at 445 nm (f=0.805), whereas no significant absorption is found in the 350-600 nm region for **TB202**. This trend is qualitatively in agreement with the experimental spectra displayed in Figure 1a. To obtain more quantitative theory-experiment comparisons, we have computed 0-0 energies, which are 1.576 eV and 1.461 eV for **TB179** and **TB202**, respectively, which compares well to 1.66 eV and 1.56 eV values displayed in Table 1. The frontier MOs and the electronic density difference

(EDD) plots of the two dyes are displayed in Figure 2. For both cases, the MOs are well-delocalized over the core with noticeable contributions from the side thienyl rings. The EDDs indicate that the density reorganization is centred on the core, with alternating zones of density gain and loss with a slight donating character of the thienyl groups but small contributions of the cyano groups. Finally, in the DFT calculations, the HOMO is upshifted by 0.158 eV when replacing the fluorine atoms by phenyl groups, whereas the LUMO is increased by a similar value (+0.150 eV). The former value follows the measured electrochemical trends.

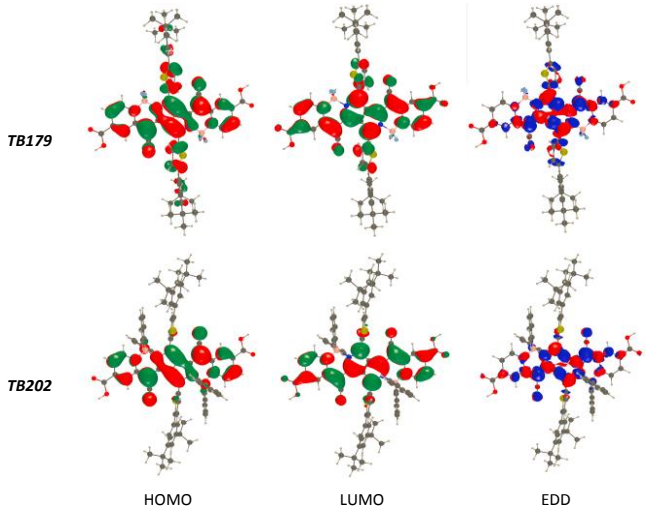

Figure 2. Representation of the frontier molecular orbitals (0.02 au) and electron density difference plots (0.0005 au) for the two compounds **TB179** and **TB202**. In the latter the blue and red zones correspond to decrease and increase of density upon absorption, respectively.

Photophysical measurements by ultrafast spectroscopy

In order to rationalize the relatively low J_{sc} values for **TB202** (see below), we performed femtosecond transient absorption (TAS) experiments with 50 fs excitation at 770 nm and probing in the 480-1000 nm spectral range. Since aggregates are known to quench the monomer excited states through ultrafast resonance energy transfer (ET),[37,38] we reduced the aggregate concentration by choosing a molar ratio of dye-to-CDCA of 1:100 (10 mM CDCA, fig. 1B). We performed comparative studies on DSSCs prepared with TiO_2, on one hand, where ET and charge transfer (CT) take place and, on the other hand, with high-band gap Al_2O_3 where CT is suppressed and only ET is observed. Figure 3 displays TAS spectra for selected delay times and kinetic traces at 680, 825 and 910 nm for Al_2O_3 and TiO_2 cells.

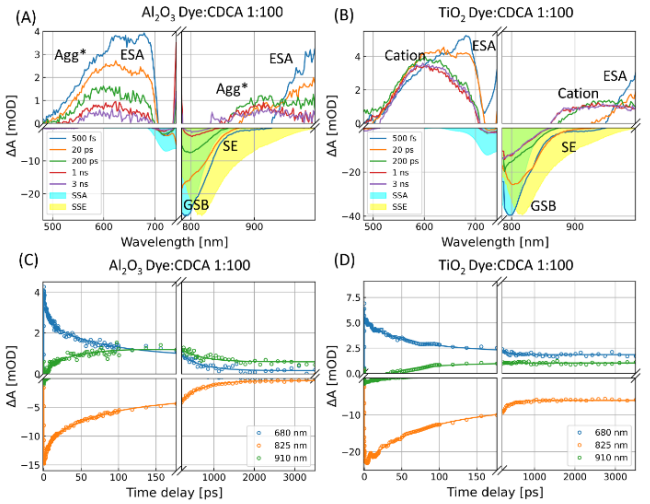

Figure 3. Transient absorption spectra of DSSCs prepared with Al_2O_3 (A) and TiO_2 (B) at different delay times. SSA: inverted steady-state absorption; SSE: inverted steady-state fluorescence. Kinetic traces are displayed at selected wavelengths for Al_2O_3 cell (C) and TiO_2 cell (D). The circles are the measured data points and the continuous lines are the fitted data. Excited state decay (680 & 825 nm) in the first 150 ps goes along with formation of the photoproducts (910 nm). Differences between Al_2O_3 and the TiO_2 cells can be found in the long-time behaviour: Agg* decays but the cation absorption remains stable.

Guided by the signatures for excited state decay in **TB202** solution (see the SI), excited state absorption (ESA) and stimulated emission (SE) are identified for both DSSCs with maxima at 680 and 1000 nm (ESA, $\Delta A>0$) and 820 nm (SE, $\Delta A<0$), respectively. They are clearly present in the spectra at 0.5 and 20 ps, in addition to ground state bleach (GSB, $\Delta A<0$) at 795 nm. At later times signatures of the photoproducts dominate the positive differential absorption. In the TiO_2 DSSC (Figure 3b), the absorption of the (**TB202**$^+$) cation is characterized by a broad absorption in the 520-700 nm range, with a maximum at 580 nm, and a weaker flat band ranging from 870 nm into the near-IR. At 200 ps, these bands are fully formed and they do not decay on longer time scales. In contrast, for Al_2O_3 the ESA and SE decay give rise to weak absorption bands in the VIS (max. 600 nm) and in the near-IR (max. 910 nm), which we assign to absorption from aggregates (Agg*) excited through ET, possibly leading to an intra-aggregate CT state.[39] These spectral features should also show up in the TiO_2 DSSC, but since they overlay spectrally with the cation absorption, they are difficult to resolve. However, contrary to the cation absorption, Agg* decays on a time scale of hundreds of ps.

In order to capture the relevant lifetimes for CT and ET, we performed a global analysis of the data, under the assumption that the kinetics are described by sets of few wavelength-independent time constants using the VARPRO algorithm.[40,41] Satisfactory fits are obtained with a minimum of four decay times, in addition to a non-decaying (> 3.5 ns = ∞) component (see Figure 3c & D and Figure S6 for the results at selected wavelengths). The result of the global fitting procedure is the decay-associated difference spectra (DADS) displayed in Figure S5. They allow us to assign the different time constants to the

relevant excited state processes. These results are summarized in the proposed reaction scheme displayed in Figure 4.

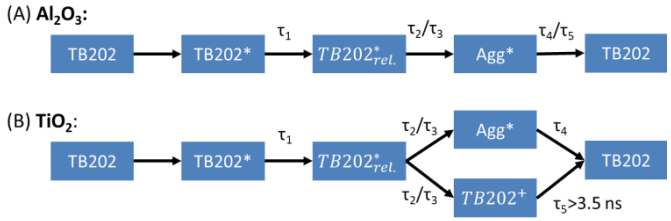

Figure 4. Proposed reaction scheme for Al_2O_3 cell (A) and TiO_2 cell (B). The excited TB202 decays into a relaxed state on a τ_1 time scale. For Al_2O_3 τ_2 and τ_3 indicate the range of timescales on which ET occurs. The Agg* state decays within τ_4 and τ_5. For the TiO_2 cell, the τ_2 and τ_3 components can be associated with ET and the cation formation (CT). The latter has a lifetime > 3.5 ns.

For both TiO_2 and Al_2O_3, τ_1 (0.3-0.4 ps) is mainly due to exc. state relaxation (spectral shift of SE and ESA). For Al_2O_3 excited state features (ESA and SE) decay during τ_2=4.4 ps and τ_3=55 ps, and Agg* (neg. comp. @880-950 nm) rises, meaning that the monomer-to-aggregate ET occurs on these time scales. Due to structural heterogeneity and the statistical distribution of monomer-to-aggregate distances and relative orientations, the ET times cover in reality a large range of values, characterised within the global fitting approach by the representative values of τ_2 to τ_3[20]. The dependence of the lifetimes and their amplitudes on the CDCA concentration is summarized in Table S2. The excited aggregates (Agg*) with absorption bands in the VIS (500-700 nm) and near-IR (850-1000 nm) decay during τ_4 (0.5 ns) and τ_5 (> 3.5 ns) time scales back to the ground state. For TiO_2, τ_2 (2.8 ps) and τ_3 (47 ps) are the time scales of excited state decay and rise of both the cation and the Agg* absorption, as indicated by the small neg. amplitudes at 520-630 nm, and at 850-980 nm. Indeed, the latter is responsible for the rise of the absorption at 910 nm (fig. 3D). Since the cation and Agg* absorption bands overlay both in the visible and the near-IR, and because τ_2 and τ_3 are very similar to the ET time scales in Al_2O_3, we conclude that both CT and ET occur in parallel on these time scales. At later times, τ_4 is the Agg* decay, and τ_5> 3.5 ns is the stable cation diff. spectrum in agreement with the long delay spectra in fig. 3B.

As pointed out above, it turns out that for **TB202** CT and ET occur on the same time scales. It is interesting to note that for TiO_2, the DADS amplitude of τ_3 is almost twice as large as for τ_2 (at 520-630 nm and 900-950 nm), meaning that approximately 2/3 of monomers release electrons only within $\tau_3 \approx 50$ ps. This is contrast to our former report of the best performing dye **TB207**,[20] where CT occurred dominantly on the sub-10 ps time scale, and faster than ET. The slower CT kinetics in **TB202** are attributed to the smaller injection driving force $\Delta G°_{inj}$= -0.02 eV for this dye (Table 2).

The TAS data allow evaluating the injection yield, defined by the ratio $\eta_{inj} = \frac{molar\ concentration\ converted\ into\ anions}{concentration\ of\ excited\ molecules}$, which one can approximate by $\eta_{inj} = \frac{GSB\ (t \gg \tau_3)}{GSB\ (t \approx 0)}$, since the ground state bleach (GSB) amplitude is given by the concentration of molecules missing in the ground state[18]. Depending on the assumptions made for the decomposition of the ΔA spectra (GSB, SE and cationic absorption), we conclude that for TB202 in a 10 mM CDCA TiO_2 device η_{inj} = 40 ± 10 %, meaning that ≈60% of monomers are de-excited through energy transfer. The injection yield is clearly lower than for TB207, for which we found η_{inj} = 65 ± 10 %. [20]

Photovoltaic characterizations

The DSSCs sensitized with *PPcy-th* **TB179** and **TB202** dyes give very low PCE with CDCA free sensitization solution (Figure S4, Table S1). By contrast to the previously reported **TB207**, but similar to the **TB144** *PPcy*- sensitizers, **TB179** and **TB202** dyes require a 1/500 ratio of dye/CDCA in order to achieve the best performances, 0.6% and 1.5% PCE, respectively, indicating that these structures are prone to form more harmful aggregation in the self-assembled monolayer (Figure 5, Table 3). We highlight here the effect of the phenyl group substitution on boron, which helps mitigating aggregations for **TB202** dye, as revealed by its higher J_{sc} (6.8 mA/cm²) than in **TB179** (4.4 mA/cm²).

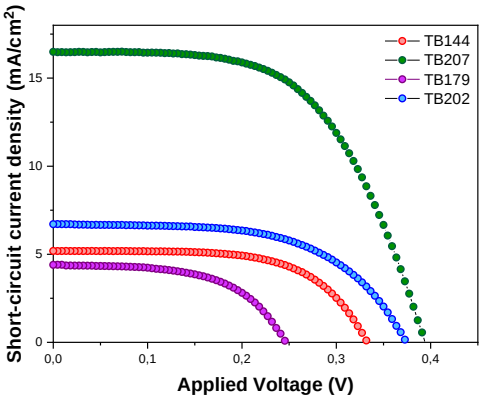

Figure 5. Evolution of J-V curves at the optimized CDCA concentration of the different PPcy and *PPcy-th* dyes: **TB144** (red), **TB207** (green), **TB179** (purple), and **TB202** (blue).

Table 3. Photovoltaic parameters of the different *PPcy* (**TB144** and **TB207**) and *PPcy-th* (**TB179** and **TB202**) dyes with optimized CDCA concentration conditions.

Dye	CDCA (mmol/L)	J_{sc} (mA/cm^2)	V_{oc} (mV)	FF	PCE (%)
TB144[20]	50	5.2	333	0.62	1.2
TB207[20]	5	16.5	394	0.58	3.8
TB179	50	4.4	246	0.56	0.6
TB202	50	6.8	367	0.58	1.5

For a more detailed understanding of the structural modification effect on the photovoltaic performances, intensity-modulated photovoltage/photocurrent spectroscopies (IMVS/PS) and dark charge extraction experiments were performed for both *PPcy* and *PPcy-th* dyes in their optimal conditions. The IMVS results presented in

Figure 6a highlight two main outcomes relative to the original structural modifications. First, they show that the *PPcy* dyes **TB144** and **TB207** exhibit a longer electron lifetime than the related *PPcy-th* **TB179** and **TB202**. The second result is that the substitution of fluorine (**TB144** and **TB179**) by phenyl (**TB207** and **TB202**) on the boron atom results in longer electron lifetimes. This is attributed to the role played by the bulkier phenyl groups as a barrier between the triiodide in the electrolyte and the injected electron in TiO_2, thus reducing the non-geminate recombination (between the injected electrons and the oxidized species in the electrolyte). The transport time is also affected by the dye structural modification, but this effect is rather small except for **TB202,** which shows a one-order of magnitude faster transport time (Figure 6b). These data allow us to evaluate charge collection efficiency of 59% for **TB179,** 97% for **TB202**, 87% for **TB144**, and 81% for **TB207**. The trap energies are affected by the structural modifications as observed from the dark charge experiments shown in Figure 6c. This is attributed to the different dipole moments of the dye on the surface of TiO_2, which hints that the dye geometry in the self-assembled monolayer is different depending on the substitution, *e.g.*, the introduction of a bulkier phenyl group to hamper aggregation. The results suggest a trend of a downshift in the surface states upon the substitution of fluorine (**TB144** and **TB179**) with phenyl (**TB202** and **TB207**). These results are in agreement with the open-circuit photovoltage recorded for these dyes, explaining the higher V_{oc} measured with phenyl *PPcy* than *PPcy-th* and when boron is substituted by phenyl. For instance, the low V_{oc} value of 246 mV measured in **TB179** devices is a result of the faster non-geminate recombination, and a downshift in the surface states.

Considering **TB202** as the best *PPcy-th*, and comparing it to the previously reported analogous *PPcy* **TB207**, the aesthetics stand out for the **TB202**-based DSSCs with the conventional triiodide/iodide redox couple. Figure 7a shows the transmittance spectra of full the DSSC (with Pt-free ITO as the counter-electrode) built from both **TB202** and **TB207** dyes. The devices are based on a 6 µm TiO_2 electrode, which was the optimized thickness to achieve the best PCE. Interestingly, an enhancement in transparency is achieved for **TB202** dye compared to **TB207**-based one, thanks to a further redshift in the absorption and smaller overlap with the photopic response range. A 63% AVT was measured for the **TB207** DSSC, while a 4% increase was observed for **TB202** device, achieving a 67% AVT. The color properties were also evaluated for the abovementioned devices, and are represented in the CIE1931 color diagram in Figure 7b.

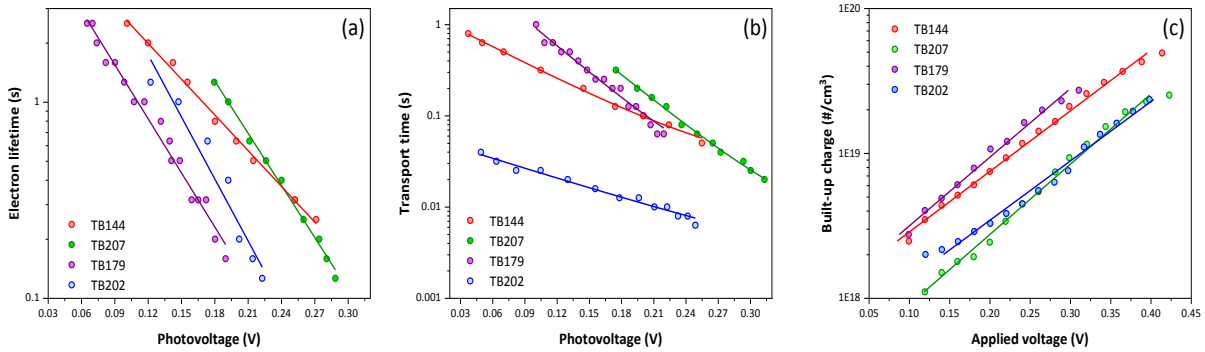

Figure 6. Evolution of (a) electron lifetime deduced from IMVS, (b) transport time deduced from IMPS, and (c) dark charge extraction measurements on NIR-DSSC based on the *PPcy* and *PPcy-th* dyes **TB144** (red), **TB207** (green), **TB179** (purple) and **TB202** (blue).

The calculations of color rendering index (CRI), chromaticity coordinates (x,y), dominant wavelength and color saturation are explained elsewhere.[9] The **TB207**-DSSC has a CRI of 82, with a dominant wavelength of 569 nm and a 38% color saturation (x= 0.3706, y= 0.4184). On the other hand, **TB202**-DSSC shows an excellent CRI of 92, with a different color dominated by 574 nm of a 40% color saturation (x = 0.388, y = 0.4132). These results suggest that the *PPcy-th* dye **TB202** is promising to achieve higher transparency for DSSCs with minimal coloration, highlighting the importance of the caused red-shift by the intended thienyl substitution.

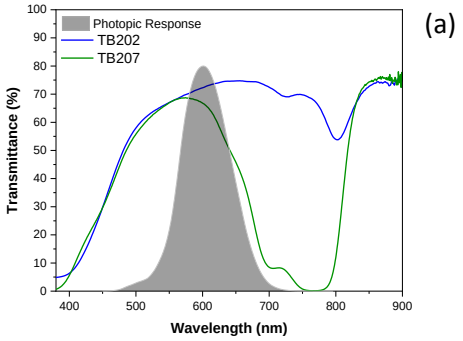

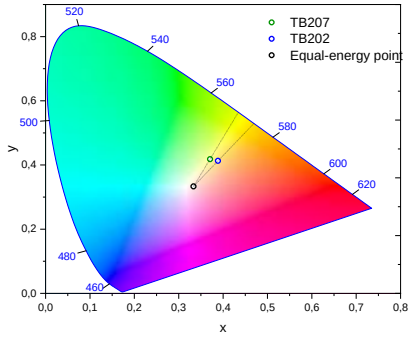

(b)

Figure 7. a) Comparison of the transmittance spectrum of **TB207** (green) and **TB202** (blue) -based NIR-DSSC. The shaded grey area represents the photopic response, b) CIE1931 x,y chromaticity diagram with the position of **TB207**-based DSSC (green point) and **TB202**-based DSSC (blue point) with triiodide/iodide electrolyte and 6 µm TiO_2. The black point is the equal energy point. The lines show the extension from the equal energy point to the coordinates of each device to the periphery of the diagram indicating the dominating wavelength.

Conclusion

In conclusion, we successfully synthesized new derivatives from pyrrolopyrrole cyanine dyes **TB179** and **TB202** bearing thiophene moieties on the bispyrrole core. In line with our expectations, this structural modification leads to a 30 nm bathochromic shift of the main absorption band, reaching 789 nm for **TB202** making them more transparent in the visible region. Unfortunately, *PPcy-th*-based DSSCs exhibit lower power conversion efficiencies than their parent phenyl *PPcy* **TB144** and **TB207**. Both the Jsc and Voc drop observed for *PPcy-th* dyes can reasonably be attributed to: i) a stronger aggregation tendency induced by the lower bulkiness of thienyl than phenyl; ii) lower injection yield hindered by a slower electron injection rate constant connected with a lower LUMO energy (less reductive in the excited state) and higher quenching by energy transfer towards the aggregates and iii) lower electron lifetime in TiO_2 that indicates more charge recombination. However, as a consequence of the redshifted absorption, **TB202** displays an improved aesthetics compared to **TB207**, reaching 67% AVT**,** and *PPcy-th* emerged as promising dyes for the development of highly colourless panels for TPV applications once the above limitations are circumvented, for example by introducing a different substitution pattern on the *PPcy* core to avoid π-π stacking with electron-rich substituents to increase the reducing ability of the dye excited state.

Author Contributions

Thibaut Baron synthesized of all the compounds described in this study and recorded the spectroscopic and electrochemical properties of the dyes and made preliminary photovoltaic measurements.

Waad Naim fabricated and optimized TB-sensitized NIR-DSSCs, did photovoltaic and optical characterization, IMVS/PS and ps-transient absorption spectroscopy measurements, and aesthetics evaluation and optimization. She synthesized and optimized the Disulfide/$CH_3SO_3S^-$ electrolyte for NIR-DSSC applications.

Mate Kurucz & Ilias Nikolinakos: fabricated TB-sensitized DSSCs, carried out the experiments on ultrafast spectroscopy on them and analysed the data.

Baptiste Andrin synthesized new batches of **TB202** for complementary characterizations.

Yann Pellegrin supervised Thibaut Baron for the spectroscopic and preliminary photovoltaic characterizations of the dyes.

Denis Jacquemin made all the quantum chemical calculations.

Stefan Haacke: supervised Ilias Nikolinakos and Mate Kurucz for the ultrafast spectroscopy.

Frédéric Sauvage coordinated VISION-NIR and IMPRESSIVE projects. He supervised Waad Naim for the optimization of the optical and performances of the TB-sensitized NIR-DSSC, device characterization with IMVS/IMPS, ps-transient absorption spectroscopy and new electrolytes.

Fabrice Odobel ignited the investigations of thienyl-*PPcy* as NIR sensitizers for TPV DSSC and supervised Thibaut Baron for the synthesis of the dyes.

Conflicts of interest

The authors declare no conflict of interest.

Acknowledgements

We acknowledge financial support by Agence National de la Recherche (ANR) through the program Vision-NIR (ANR17-CE05-0037-02) and for the EUR project LUMOMAT. S.F. acknowledges the "IMPRESSIVE" project which received funding from the European Union's Horizon2020 research and innovation program under grant agreement number no.826013. S.H. acknowledges funding provided by the ITI 2021-28 program of the University of Strasbourg, CNRS and Inserm, supported by IdEx Unistra (ANR 10 IDEX 0002), by SFRI STRAT'US project (ANR 20 SFRI 0012) and EUR QMAT ANR-17-EURE-0024 under the framework of the French "Investments for the Future" Program. D.J. acknowledges the CCIPL/Glicid computational center installed in Nantes for the generous allocation of computational resources. The authors greatly acknowledge J. Hémez and L. Arzel (AMaCC platform, CEISAM UMR CNRS 6230, University of Nantes) for the mass spectrometry analyses.

Notes and references

1 M. V. Dambhare, B. Butey and S. V. Moharil, *J. Phys.: Conf. Ser.*, 2021, **1913**, 012053.
2 A. K. Shukla, K. Sudhakar and P. Baredar, *Energy and Buildings*, 2017, **140**, 188–195.
3 K. Lee, H.-D. Um, D. Choi, J. Park, N. Kim, H. Kim and K. Seo, *Cell Reports Physical Science*, 2020, **1**, 100143.
4 E. Ravishankar, M. Charles, Y. Xiong, R. Henry, J. Swift, J. Rech, J. Calero, S. Cho, R. E. Booth, T. Kim, A. H. Balzer, Y. Qin, C. Hoi Yi

Ho, F. So, N. Stingelin, A. Amassian, C. Saravitz, W. You, H. Ade, H. Sederoff and B. T. O'Connor, *Cell Reports Physical Science*, 2021, **2**, 100381.
5 C. Tuchinda, S. Srivannaboon and H. W. Lim, *Journal of the American Academy of Dermatology*, 2006, **54**, 845–854.
6 C. Yang, D. Liu, M. Bates, M. C. Barr and R. R. Lunt, *Joule*, 2019, **3**, 1803–1809.
7 C. Yang, D. Liu, M. Bates, M. C. Barr and R. R. Lunt, *Joule*, 2019, **3**, 1803–1809.
8 C. J. Traverse, R. Pandey, M. C. Barr and R. R. Lunt, *Nat Energy*, 2017, **2**, 849–860.
9 F. Grifoni, M. Bonomo, W. Naim, N. Barbero, T. Alnasser, I. Dzeba, M. Giordano, A. Tsaturyan, M. Urbani, T. Torres, C. Barolo and F. Sauvage, *Advanced Energy Materials*, **n/a**, 2101598.
10 A. Hagfeldt, G. Boschloo, L. Sun, L. Kloo and H. Pettersson, *Chem. Rev.*, 2010, **110**, 6595–6663.
11 T. Kinoshita, K. Nonomura, N. Joong Jeon, F. Giordano, A. Abate, S. Uchida, T. Kubo, S. I. Seok, M. K. Nazeeruddin, A. Hagfeldt, M. Grätzel and H. Segawa, *Nat Commun*, 2015, **6**, 8834.
12 K.-L. Wu, S.-T. Ho, C.-C. Chou, Y.-C. Chang, H.-A. Pan, Y. Chi and P.-T. Chou, *Angewandte Chemie International Edition*, 2012, **51**, 5642–5646.
13 C. Aumaitre, C. Rodriguez-Seco, J. Jover, O. Bardagot, F. Caffy, Y. Kervella, N. López, E. Palomares and R. Demadrille, *J. Mater. Chem. A*, 2018, **6**, 10074–10084.
14 M. Godfroy, J. Liotier, V. M. Mwalukuku, D. Joly, Q. Huaulmé, L. Cabau, C. Aumaitre, Y. Kervella, S. Narbey, F. Oswald, E. Palomares, C. A. G. Flores, G. Oskam and R. Demadrille, *Sustainable Energy Fuels*, 2021, **5**, 144–153.
15 J. Luo, M. Xu, R. Li, K.-W. Huang, C. Jiang, Q. Qi, W. Zeng, J. Zhang, C. Chi, P. Wang and J. Wu, *J. Am. Chem. Soc.*, 2014, **136**, 265–272.
16 M. F. Shah, A. Mirloup, T. H. Chowdhury, S. Alexandra, A. S. Hanbazazah, A. Ahmed, J.-J. Lee, N. Leclerc, M. Abdel-Shakour and A. Islam, *Sustainable Energy Fuels*, 2019, **3**, 2983–2989.
17 K. Zhang, C. Qin, X. Yang, A. Islam, S. Zhang, H. Chen and L. Han, *Advanced Energy Materials*, 2014, **4**, 1301966.
18 W. Naim, V. Novelli, I. Nikolinakos, N. Barbero, I. Dzeba, F. Grifoni, Y. Ren, T. Alnasser, A. Velardo, R. Borrelli, S. Haacke, S. M. Zakeeruddin, M. Graetzel, C. Barolo and F. Sauvage, *JACS Au*, 2021, **1**, 409–426.
19 T. Baron, X. Zarate, Y. Hidalgo-Rosa, M. Zambrano-Angulo, K. Mall-Haidaraly, R. Pino-Rios, Y. Pellegrin, F. Odobel and G. Cárdenas-Jirón, *Comptes Rendus. Chimie*, 2021, **24**, 1–14.
20 T. Baron, W. Naim, I. Nikolinakos, B. Andrin, Y. Pellegrin, D. Jacquemin, S. Haacke, F. Sauvage and F. Odobel, *Angewandte Chemie International Edition*, 2022, **61**, e202207459.
21 A. B. Pun, L. M. Campos and D. N. Congreve, *J. Am. Chem. Soc.*, 2019, **141**, 3777–3781.
22 M. Grzybowski and D. T. Gryko, *Advanced Optical Materials*, 2015, **3**, 280–320.
23 Q. Zhang, P. Yu, Y. Fan, C. Sun, H. He, X. Liu, L. Lu, M. Zhao, H. Zhang and F. Zhang, *Angewandte Chemie*, 2021, **133**, 4013–4019.
24 K. Yang, T. He, X. Chen, S. Z. D. Cheng and Y. Zhu, *Macromolecules*, 2014, **47**, 8479–8486.
25 G. M. Fischer, M. Isomäki-Krondahl, I. Göttker-Schnetmann, E. Daltrozzo and A. Zumbusch, *Chemistry – A European Journal*, 2009, **15**, 4857–4864.
26 A. Loudet and K. Burgess, *Chem. Rev.*, 2007, **107**, 4891–4932.
27 R. Gresser, M. Hummert, H. Hartmann, K. Leo and M. Riede, *Chemistry – A European Journal*, 2011, **17**, 2939–2947.
28 G. M. Fischer, M. K. Klein, E. Daltrozzo and A. Zumbusch, *European Journal of Organic Chemistry*, 2011, **2011**, 3421–3429.
29 D. Kumaresan, R. P. Thummel, T. Bura, G. Ulrich and R. Ziessel, *Chemistry – A European Journal*, 2009, **15**, 6335–6339.
30 L. Zhang and J. M. Cole, *J. Mater. Chem. A*, 2017, **5**, 19541–19559.
31 V. S. Manthou, E. K. Pefkianakis, P. Falaras and G. C. Vougioukalakis, *ChemSusChem*, 2015, **8**, 588–599.
32 G. M. Fischer, M. K. Klein, E. Daltrozzo and A. Zumbusch, *European Journal of Organic Chemistry*, 2011, **2011**, 3421–3429.
33 E. M. Espinoza, J. A. Clark, J. Soliman, J. B. Derr, M. Morales and V. I. Vullev, *J. Electrochem. Soc.*, 2019, **166**, H3175.
34 A. B. Nepomnyashchii and A. J. Bard, *Acc. Chem. Res.*, 2012, **45**, 1844–1853.
35 M. Grätzel, *Acc. Chem. Res.*, 2009, **42**, 1788–1798.
36 A. Y. Anderson, P. R. F. Barnes, J. R. Durrant and B. C. O'Regan, *J. Phys. Chem. C*, 2011, **115**, 2439–2447.
37 M. Ziółek, J. Karolczak, M. Zalas, Y. Hao, H. Tian and A. Douhal, *J. Phys. Chem. C*, 2014, **118**, 194–205.
38 K. Pydzińska and M. Ziółek, *Dyes and Pigments*, 2015, **122**, 272–279.
39 H.-W. Bahng, A. Hagfeldt and J.-E. Moser, *J. Phys. Chem. C*, 2018, **122**, 19348–19358.
40 D. P. O'Leary and B. W. Rust, *Comput Optim Appl*, 2013, **54**, 579–593.
41 G. H. Golub and V. Pereysa, in *Generalized Inverses and Applications*, ed. M. Z. Nashed, Academic Press, 1976, pp. 303–324.